RESEARCH COMMUNICATION

Biofactors WILEY

Rapid and simultaneous determination of histidine metabolism intermediates in human and mouse microbiota and biomatrices

Inmaculada Acuña[1,2] [ORCID] | Alicia Ruiz[3] | Tomás Cerdó[4] | Samuel Cantarero[5] |
Ana López-Moreno[2,6] | Margarita Aguilera[2,6,7] [ORCID] | Cristina Campoy[8,9] |
Antonio Suárez[1,2]

[1]Department of Biochemistry and Molecular Biology 2, Biomedical Research Centre, University of Granada, Granada, Spain

[2]Instituto de Nutrición y Tecnología de los Alimentos, INYTA, Biomedical Research Centre, University of Granada, Granada, Spain

[3]Centre for Inflammation Research, Queen's Medical Institute, University of Edinburgh, Edinburgh, UK

[4]Carlos III Health Institute, Madrid, Spain

[5]Centre for Scientific Instrumentation, University of Granada, Campus of Fuentenueva, Granada, Spain

[6]Department of Microbiology, Faculty of Pharmacy, University of Granada, Campus of Cartuja, Granada, Spain

[7]Instituto de Investigación Biosanitaria, Ibs-Granada, Granada, Spain

[8]Department of Paediatrics, School of Medicine, University of Granada, Granada, Spain

[9]Spanish Network of Biomedical Research in Epidemiology and Public Health (CIBERESP), Granada's node, Institute of Health Carlos III, Madrid, Spain

Correspondence
Antonio Suárez, Department of Biochemistry and Molecular Biology 2, Biomedical Research Centre, University of Granada, 18016, Granada, Spain.
Email: asuarez@ugr.es

Abstract

Histidine metabolism is a key pathway physiologically involved in satiety, recognition memory, skin, and neural protection and allergic diseases. Microbiologically-produced imidazole propionate induces type II diabetes and interferes with glucose lowering drugs. Despite their determinant health implications, no single method simultaneously assesses histidine metabolites in urine, feces, and microbiota. The aim of this study was to develop a simple, rapid, and sensitive method for the determination of histidine and its major bioactive metabolites histamine, N-acetylhistamine, imidazole-4-acetate, cis-urocanate, trans-urocanate, glutamate and imidazole propionate, using ultrahigh-performance liquid chromatography with electrospray ionization tandem mass spectrometry. An innovative simple extraction method from small aliquots of human and mice urine, feces and

Abbreviations: ACN, acetonitrile; ATAA, 2-amino-4-thiazoleacetic acid; FDA, US Food and Drugs Administration; GSH, reduced glutathione; HAL, histidine ammonia-lyase; HDC, histidine decarboxylase; HF, human feces; HM, human microbial metabolome; HU, human urine; IS, internal standards; LOD, limit of detection; LOQ, limit of quantification; ME, matrix effects; MF, mouse feces; MM, mouse microbial metabolome; MRM, multiple reaction monitoring mode; MU, mouse urine; PBS, phosphate saline buffer; P_{lof}, probability level of the lack-of-fit test; Rec, recovery rates; RSD, relative standard deviation; UHPLC–ESI–MS/MS, ultrahigh-performance liquid chromatography with electrospray ionization tandem mass spectrometry; UV, ultraviolet.

Inmaculada Acuña, Alicia Ruiz, and Tomás Cerdó contributed equally to this work.

microbial cell extracts was coupled to separation in a 6.5 min chromatographic run. The successful performance allowed accurate and precise quantification of all metabolites in mouse feces, suggesting broad exchange of histidine metabolites between the gut and mice. Higher urine histamine, histamine to histidine ratio, and imidazole-4-acetate pointed to an underlying inflammatory or allergic process in mice compared to human subjects. N-acetylhistamine and imidazole propionate were detected in human and mouse feces, confirming its origin from gut microbial metabolism. Our novel and robust analytical method captured histidine metabolism in a single assay that will facilitate broad and deep histidine metabolic phenotyping assessing the impact of microbiota on host health in large-scale human observational and interventional studies.

1 | INTRODUCTION

The gut microbiota is a dense and diverse microbial community present in the gastrointestinal tract composed approximately by 10^{14}–10^{15} bacterial cells (i.e., 10 times the number of eukaryotic cells in the body), largely contributing to organism health and disease in terms of their relative genetic content. Extensive evidence has revealed that gut microbial communities have co-evolved with the host to develop a mutualistic relationship, influencing metabolic homeostasis, endocrine system, brain function, and macronutrient availability.[1] Gut microbiota modulate several processes along the gastrointestinal tract; playing an important role in the extraction, synthesis, and absorption of many nutrients and metabolites, including bile acids, lipids, short-chain fatty acids, vitamins, and amino acids.[2] Indeed, more than 50% of the metabolites present in feces and urine are derived from or modified by the gut microbiota.[3] Specifically, the gut microbiota is not only involved in amino acid synthesis or fermentation but in the regulation of amino acid catabolism, even providing unique forms of amino acid modification that yield by-products with immune, metabolic, and neurologic impact.[4–6]

Such chemical crosstalk between the host and its gut microbiota may also reach histidine metabolism. Histidine is a nutritionally essential amino acid in mammals, fish, and poultry because it is not de novo synthesized and must be obtained through the diet.[7,8] Histidine plays an important role in anemia, erythropoiesis, hemoglobin metabolism, skin lesion, malaise, anorexia, and mental charge,[9] and has been shown to improve insulin sensitivity, induce body fat loss with reduction of waist circumference, reduce appetite, and decrease oxidative stress and plasma levels of systemic inflammation markers.[10]

Dysfunction of the histidine pathway has been linked to vascular, dermatological, metabolic, digestive, immunological, and neurological disorders (Figure 1). Histamine is a biogenic amine synthesized from histidine by the action of histidine decarboxylase (HDC). Histamine is a neurotransmitter with roles in gastric secretions and colonic motility and in multiple central nervous system disorders including insomnia, narcolepsy, Parkinson's disease, schizophrenia, Alzheimer's disease, and cerebral ischemia. Additionally, histamine shows both pro-inflammatory and anti-inflammatory effects on immunoregulatory processes and is a major mediator in allergic diseases.[11–14] Histamine is further oxidized to imidazole-4-acetate, a γ-aminobutyric acid-type A receptor agonist, and type C receptor antagonist, whose administration to animals reduces motor activity, enhances seizures, and allodynia and leads to a sleep-like state with seizures.[15–18] Histamine can alternatively progress to N-acetylhistamine which acts as a powerful stimulant of gastric secretion, a constrictor of bronchial smooth muscle, a regulator of body temperature, a vasodilator and a centrally acting neurotransmitter.[19] Excess of dietary histidine is irreversibly degraded to *trans*-urocanate by the rate-limiting action of histidine ammonia-lyase (HAL) or histidase, an enzyme highly expressed in the surface layer (stratum corneum) of the skin and in the liver.[20] *Trans*-urocanate can be an important intermediary in the histidine to glutamate metabolic pathway that has been associated with increased excitatory neurotransmission.[21] In the skin, *trans*-urocanate serves as a natural sunscreen since photoisomerization to *cis*-urocanate absorbs UV radiation.[22] Many in vivo and in vitro studies have revealed the local and systemic anti-inflammatory and immunosuppressive properties of *cis*-urocanate, downregulating hypersensitivity reactions, suppressing cell mediated immunity, attenuating
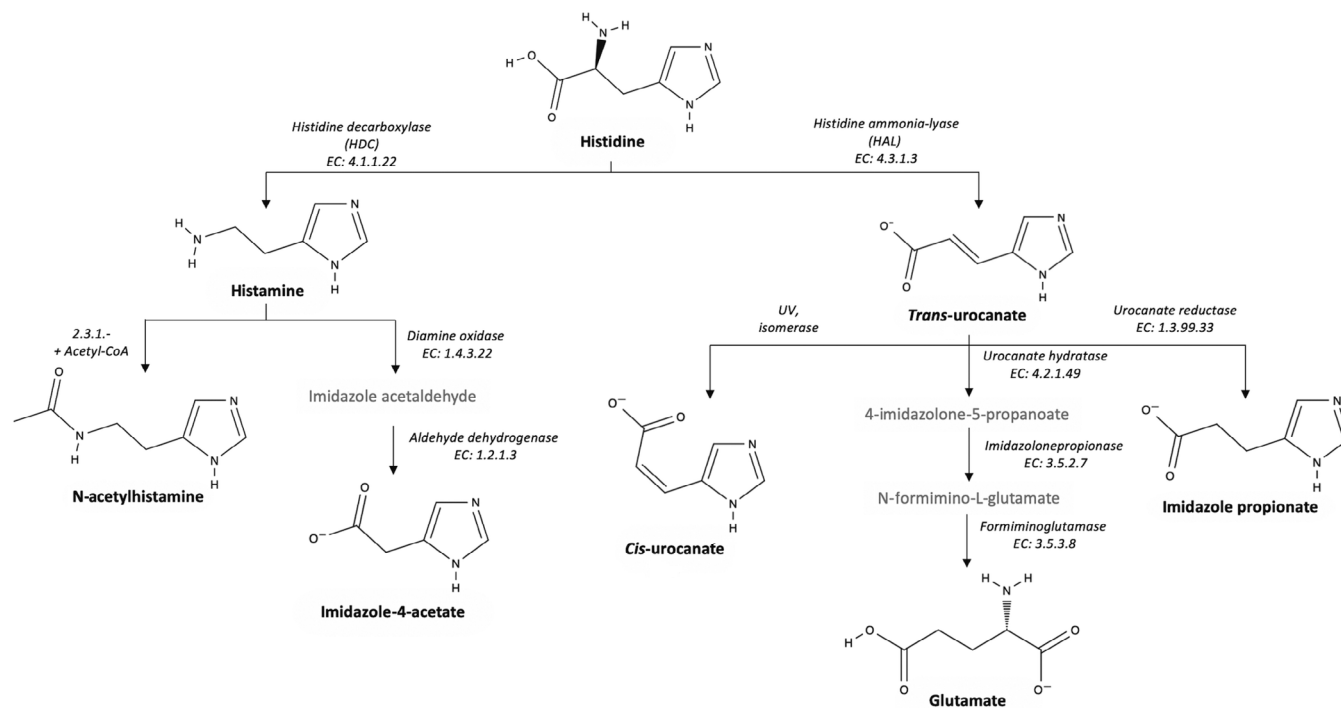
FIGURE 1 Metabolic pathways involving measured metabolites from the histidine metabolism

sclerosis, and dextran sulfate-induced inflammatory bowel disease and protecting cells from UV injury.[23–26] In the liver, after two reaction steps, *trans*-urocanate is finally converted into glutamate, a non-essential amino acid with vital roles in intermediary metabolism and in the biosynthesis of nucleic acids, proteins and amino acids such as proline and arginine. Glutamate, the most abundant amino acid in the mammalian brain, acts as a major excitatory neurotransmitter through a wide variety of receptors regulating neuroimmune crosstalk, language, synaptic plasticity, learning, memory, motor activity, neural development, and Alzheimer's disease.[27–31] Last but not least, *trans*-urocanate can also be reduced to imidazole propionate (dihydrourocanate or deamino-histidine) by urocanate reductase, a metabolic route provided by gut microbiota to mammals. Recently, microbially-produced imidazole propionate has been shown to be elevated in plasma of prediabetic and type-2 diabetic subjects, induce type-2 diabetes via mTORC1 and reduce glucose-lowering effects of metformin.[32–34]

Despite the physiological importance of histidine and its bioactive metabolites, the lack of a standardized and sensitive method for their simultaneous detection and quantification hampers correct assessment of the influence of gut ecosystem dysbiosis in large cohort disease studies. The objective of this study was to develop a quick and effective method to quantify the concentrations of histidine and its bioactive metabolites N-acetylhistamine, glutamate, imidazole propionate, imidazole-4-acetate, *cis*-urocanate, *trans*-urocanate and histamine in feces, urine

and, specifically, in microbiota metabolome from healthy infants and C57BL/6 mice. A major achievement was the determination of histidine metabolites in a single assay because simultaneous metabolite quantitation allows accurate assessment of metabolite ratios, yielding statistically robust associations with perturbations in pathways rather than separate analyses of single metabolites.[35] The validation was carried out by spiking the sample solutions with two standards (atenolol and 2-amino-4-thiazoleacetic acid [ATAA]), undetected in human and mouse biosamples.[21,36] To fulfill our goal, we used ultrahigh-performance liquid chromatography with electrospray ionization tandem mass spectrometry (UHPLC–ESI–MS/MS) due to its ability to accurately identify and quantify multiple chemical compounds.

2 | MATERIALS AND METHODS

2.1 | Chemicals and reagents

Water (18.2 MΩ cm^{-1}) was purified with a Milli-Q Plus® system (Millipore, Madrid, Spain). The LC–MS solvent (acetonitrile, ACN) and additive (formic acid) were of UHPLC–MS-grade and were from Scharlau (Scharlab S.L., Barcelona, Spain). L-glutamate, imidazole-4-acetate, N-acetylhistamine, *cis*-urocanate, imidazole propionate and 2-amino-4-thiazoleacetic acid were from Sigma-Aldrich Chemie GmbH. *Trans*-urocanate, histamine, and atenolol were obtained from Acros Organics (Geel, Belgium).

L-histidine was from VWR International Ltd (UK). Other chemicals used for measuring enzymatic activities were BugBuster Protein Extraction Reagent (Novagen, Darmstadt, Germany), magnesium chloride, reduced glutathione, pyridoxal-5′-phosphate and aminoguanidine (Sigma-Aldrich, Chemie GmbH).

2.2 | Extraction protocol for metabolite isolation

2.2.1 | Human and mouse samples

Ten healthy full-term infants aged 6-months, who did not present any intestinal disorders and had not taken antibiotics, were chosen from the panel of infants that belonged to PREOBE study cohort.[37] Urine and fresh stools were collected at 6-months after delivery and were immediately stored at −80°C, until processing. This project followed the ethical standards recognized by the Declaration of Helsinki (reviewed in Hong-Kong 1989 and in Edinburgh 2000) and the EEC Good Clinical Practice recommendations (document 111/3976/881990), and current Spanish legislation regulating clinical research in humans (Royal Decree 561/1993). Also, urine and stool samples were collected from 10 4-week-old C57BL/6 mice. Mice received human care and all experimental protocols were approved by the institutional animal ethics committee and performed in accordance with national and institutional regulations.

2.2.2 | Urine preparation

Frozen urine samples were thawed and a 10 μL aliquot was transferred by pipetting into a 1.5 mL Eppendorf tube. Nine hundred and ninety microliters of ACN/H$_2$O (50/50; v/v) were added to urine samples. The tubes were centrifuged at 13,000 rpm at 4°C for 10 min. Urine supernatants were removed, filtered through 0.2-μm nylon syringe filters and frozen in analytical vials at −20°C until UHPLC–MS/MS analysis.

2.2.3 | Fecal and microbial intracellular metabolites

Microbiota cells were separated from the fecal matrix by mixing 0.1 g of fecal sample with 2 mL of 0.05% L-cysteine phosphate saline buffer solution. Following re-suspension (by 1 min of vigorous vortexing), the samples were then centrifuged at 500g for 1 min at 4°C to remove fecal debris. The supernatant was transferred to a 2-mL Eppendorf tube and centrifuged at 14,000g at 4°C for 1 min to pellet the cells. Five hundred microliters of this supernatant were mixed with 500 μL of UHPLC–MS-grade ACN to precipitate proteins. This solution was then centrifuged at 13,000 rpm at 4°C for 10 min to separate any solid impurities. The supernatants were removed, filtered through 0.22-μm nylon syringe filters and frozen in analytical vials at −20°C until UHPLC–MS/MS analysis.

Pelleted microbiota cells were resuspended in 300 μL of phosphate saline buffer solution (PBS) and split into two aliquots. For determination of intracellular histidine bioactive metabolites, microbial cells were lysed with 15 consecutive freeze–thaw cycles in liquid nitrogen and a thermoblock (28°C). The samples were sonicated for 2 min on ice (Bandelin Sonopuls, HD 2070) at the 30% amplitude setting. The final pellet was removed following centrifugation at 14,000g for 10 min at 4°C. Supernatants were mixed with 150 μL of UHPLC–MS-grade ACN, and centrifuged at 13,000 rpm for 10 min at 4°C. The supernatants were removed, filtered through 0.2-μm nylon syringe filters and frozen in analytical vials at −20°C until UHPLC–MS/MS analysis.

2.3 | Measurement of microbial HAL and HDC activities

The remaining aliquot of resuspended microbiota cells was mixed with the same volume of BugBuster protein extraction reagent, gently shaken for 30 min at 37°C and further disrupted by freeze–thaw cycles and sonication as previously described. Protein extracts were centrifuged at 14,000g for 10 min at 4°C to separate cell debris. Product synthesis by the enzymes HAL and HDC were measured in protein extracts using 1 mg mL^{-1} histidine substrate. HAL reactions were determined in 200 mM Tris HCl buffer pH 9 with 10 mM MgCl$_2$ and 100 mM GSH. HDC reactions were measured in 80 mM sodium acetate pH 6.5 with 61 mM pyridoxal-5′-phosphate and 10 mM aminoguanidine.

2.4 | Standard solutions and calibration curves

Standard solutions were prepared individually in 1 mg mL^{-1} ACN/H$_2$O, (50/50 v/v). The same dilution solvents were used for internal standards (IS) stock solutions. Standard and IS stock solutions were stored at −20°C for up to 2 weeks. Working solutions were prepared weekly by diluting stock solutions with the same solvent.

Calibration was built by dilution of standard stock solutions in ACN/H$_2$O (50/50; v/v) to obtain six solutions

in ng mL^{-1} range for target analytes. Each point of the standard curve was prepared in triplicate and each extract was analyzed three times. IS, atenolol for urocanates and ATAA for the other analytes were added after extraction at a final concentration of 10 ng mL^{-1}. Calibration curves were plotted using analyte/internal standard peak area ratio versus concentration of analyte.

2.5 | Instrumentation and analytical conditions

A high-throughput method was developed using UHPLC–ESI–MS/MS. All measurements were completed in the Centre for Scientific Instrumentation (University of Granada). Chromatography was performed with a Waters Acquity UPLC™ System I-Class (Waters, UK). Two different ultra-performance liquid chromatography analyses were examined: (i) generic analysis, separation was performed using an Acquity UPLC HSS™ T3 (1.8 μm, 2.1 × 150 mm; Waters) column (*HSS T3 Column*); and (ii) urocanate isomer analysis, separation was carried out using an Acquity ultra-performance liquid chromatography BEH™ Amide (1.7 μm, 2.1 × 100 mm; Waters) column (*BEH Amide Column*). Instrumental parameters are shown in Table 1. In both analytical methods, mobile phase A was 0.1% formic acid in water, and the mobile phase was B 0.1% formic acid in ACN. The column was used at room temperature. The sample injection volume was 10 μL, and the flow rate was 0.3 and 0.35 mL min^{-1}, respectively. Mass spectrometry was performed with a Waters triple quadrupole mass spectrometer (XevoTQ-XS, Waters, UK). The mass spectrometer was operated in the positive ESI mode with the following operation conditions: capillary voltage, 2.90 kV; ion source temperature, 150 °C; desolvation temperature, 600 °C; desolvation gas flow rate, 500 L h^{-1}; cone gas flow rate, 150 L h^{-1}. The protonated molecular ions $[M + H]^+$ of histidine bioactive metabolites were chosen as the precursor ions, because of their highest optimization of the

TABLE 1 Transitions and optimized potentials for UHPLC–MS/MS analysis of histidine metabolites

	Chemical formula	tR (min)	Transitions	CV	CE
HSS T3 column					
Histidine	$C_6H_9N_3O_2$	0.9	156.04 → 82.33[a]	6	18
			156.04 → 92.48[b]	6	18
N-acetylhistamine	$C_7H_{11}N_3O$	1.49	154.06 → 67.38[a]	4	24
			154.06 → 94.49[b]	4	14
Glutamate	$C_5H_9NO_4$	1.05	148.02 → 101.51[a]	6	8
			148.02 → 83.43[b]	6	12
Imidazole propionate	$C_6H_7N_2O_2$	1.49	141.09 → 80.43[a]	2	18
			141.09 → 94.51[b]	2	10
Imidazole acetate	$C_5H_6N_2O_2$	1.31	127.14 → 53.30[a]	28	20
			127.14 → 80.38[b]	28	4
Histamine	$C_5H_9N_3$	0.83	112.11 → 40.31[a]	12	18
			112.11 → 82.41[b]	12	8
ATAA	$C_5H_6N_2O_2S$	1.49	159.05 → 70,33[a]	4	26
			159.05 →112.51[b]	4	22
BEH amide column					
Cis-urocanate	$C_6H_5N_2O_2$	1.5	139.07 → 65.29[a]	32	18
			139.07 → 92.48[b]	32	16
Trans-urocanate	$C_6H_5N_2O_2$	1.92	139.07 → 65.29[a]	32	18
			139.07 → 92.48[b]	32	16
Atenolol	$C_{14}H_{22}N_2O_3$	1.81	267.19 → 144.67[a]	6	26
			267.19 → 189.83[b]	6	16

Abbreviations: CV, cone voltage (V); CE, collision energy (eV).

[a]MRM transition used for qualification.

[b]MRM transition used for quantification.

instrument parameters. One specific mass transition (m/z) was selected for each analyte using the multiple reaction monitoring mode (MRM) function of the instrument for qualification and quantitation. The optimized compound-dependent mass parameters (cone voltage and collision energy) and the MRM transitions are shown in Table 1. Chromatography details of each method and MS settings are provided in the Supplementary Material, Tables S1 and S2. Masslynx software version 4.2 was used for instrument control and data acquisition. Statistical analyses were carried out using SPSS version 26.0 (IBM SPSS, Inc., Chicago, IL).

2.6 | Matrix effect and validation

To check for the matrix effect for IS and consequently for histidine bioactive metabolites, a slope comparison between several calibration curves were performed. A six-concentration-level curve for atenolol and ATAA in distilled water and ACN was prepared. Similarly, a second calibration curve was carried out by adding to every matrix the same amount of IS as used in the standard calibration (six calibration levels).

We validated the developed method in terms of linearity, limit of detection (LOD), limit of quantification (LOQ), selectivity, accuracy (trueness and precision) and recovery according to the US Food and Drugs Administration (FDA) guideline for Bioanalytical Method Validation.[38] Calibration curves were prepared by calculating the chromatographic peak area ratio of the analyte and it IS for each metabolite at each concentration level. LOD is the minimum amount of compound detectable in the sample, while the LOQ is the minimum amount quantified. Both were determined in order to check the sensitivity of the analytical method. In this work, these parameters were calculated following the method defined by Currie.[39] We extracted their values from the calibration function, using the standard deviation of residual, $S_{y/x}$, the slope of the curve, b, and an estimation of the standard deviation of the blank (S0). The LOD is defined as 3·S0 and the LOQ as 10·S0. Selectivity was assessed by comparing the chromatogram of the blank sample with the corresponding spiked sample containing a known concentration of the internal standards. Accuracy (trueness and precision) was assessed by spiking samples at low, medium, and high levels (5, 50, and 100 ng mL^{-1}, respectively) in three replicates for each compound during three consecutive days. We used solvent blanks every 10 samples to control background contamination and we did not find quantifiable amounts of target analytes.

3 | RESULTS AND DISCUSSION

Amino acids are one of the main building blocks of life and are used in a variety of metabolic and physiological forms by the gut microbiota.[40] One of these amino acids, histidine and its bioactive metabolites, have broad physiological effects ranging from neurological development and disorders to dermatologic, metabolic, digestive, vascular and immunosuppressive effects.[9–34,41] Using UHPLC–ESI–MS/MS, we developed a novel method to simultaneously determine histidine and seven bioactive metabolites easily extracted from a small amount of human and mice urine, feces and microbiota metabolome in a single rapid run (6.5 min), enabling a comprehensive assessment of organismal histidine metabolism. We also monitored activity of the main enzymes governing histidine metabolism, HAL and HDC, in gut microbial cellular extracts.

3.1 | Method optimization

We employed the UHPLC–ESI–MS/MS method due to its accuracy, selectivity, sensitivity, and reproducibility. Although the negative mode was proved, the use of positive ESI resulted in good ionization of the compounds and $[M + H]^+$ ions were selected as precursor ions. Selectivity and sensitivity of the method were further improved by the choice of the product ion producing the highest response. Different stationary phase and mobile phase options were tested, and eventually we obtained the best separation, peak shape, and response in an 0.1% formic acid in water (v/v) and an ACN mobile phase in the gradient elution mode.

We tested different C18 columns for a reverse-phase analysis, such as Acquity HSS T3 column (1.8 μm, 2.1 × 150 mm) that promotes polar compound retention and aqueous mobile-phase compatibility. When we used HSS T3 column, histidine metabolites were well retained but *cis*- and *trans*-urocanate isomers were split into two broad peaks. We then tested the hydrophilic interaction liquid chromatography (HILIC) analysis for urocanate isomer separation. We ran the analysis on the BEH amide column (1.7 μm, 2.1 × 100 mm) since this is known to provide sufficient retention for very polar compounds.[42] Separation on the HILIC column was previously tested by Joo et al., and it was successfully applied to determine the level of *cis*- and *trans*-urocanate in the stratum corneum from forearm and forehead samples.[43] We observed a sufficient separation and good peak shapes of urocanates, but displayed a poor performance for the other analytes. As improving separation of isomers without sacrificing broad coverage was one of the

key objectives in developing this method, we decided to use the HSS T3 Column to detect and quantify histidine, N-acetylhistamine, glutamate, imidazole propionate, imidazole-4-acetate and histamine, and the BEH Amide Column for *trans-* and *cis-*urocanate.

3.2 | Method validation

3.2.1 | Evaluation of matrix effect

Due to its high selectivity and sensitivity, mass spectrometry in tandem with liquid chromatography is a powerful analytical tool.[44] However, the development of HPLC-MS/MS instrumentation and its applications do not guarantee the effective elimination of interferences from endogenous impurities. Quantitative analysis with ESI can be substantially affected by the occurrence of ion-suppression or -enhancement caused by the presence of a matrix or other interferences in the sample, as reported by many authors.[44,45] This phenomenon is commonly referred as "matrix effects (ME)," and it is responsible for poor and unreliable data in a quantitative assay, inducing a heavy influence in the reproducibility, linearity and accuracy of the method.[45] Matrix effects may occur in any LC–MS analysis, especially in complex matrices such as feces, microbial metabolome and urine. The use of IS is a noted efficient strategy to overcome and ameliorate matrix effects and consequently improve the accuracy of the method.[44]

In the present work, we propose the use of two standards with similar structures and chemical behavior analogous to the histidine metabolites: atenolol[21] for *cis-* and

*trans-*urocanate, and ATAA[36] for the other metabolites. Those compounds have never been detected in human and mice samples and were not detected in our samples. We spiked these two standards in human and mouse urine (HU, MU), feces (HF, MF), and microbial metabolome (HM, MM).

To check the presence or absence of matrix effect for atenolol or ATAA standard and consequently for the histidine metabolites, a slope comparison between different calibration curves was carried out. First, a six-concentration-level curve for atenolol and ATAA in distilled water and ACN was prepared. In a similar way, a second calibration curve was performed by adding to every matrix the same amount of atenolol and ATAA as used in the standard calibration (six calibration levels). Tables 2 and 3 show the obtained calibration parameters.

A *t*-Student test was applied to compare the statistical similarity between the values of the slope for each calibration curve.[46] First, we compared the variances, estimated as $s_{y/x}^2$ by means of the Snedecor's F distribution. The calculated F-values were lower than the critical F value of 6.38 (significance level 5% and 4 degrees of freedom), and variances were equal. Consequently, the calculated t value is obtained with the equation

$$t_{cal} = (b_1 - b_2)/\sqrt{(s_{b1}^2 + s_{b2}^2)}$$

where b_1, b_2, s_{b1}^2 and s_{b2}^2 are the slopes of the calibration curves and their respective variances. These values were compared with the theoretical *t*-value of 2.23 and were lower, indicating no significant differences in the slopes and intercepts. As the response for both standards was statistically equal, in deionized water + ACN and in

TABLE 2 Matrix effect. Comparison of calibration curves in H_2O + ACN (standard) and every of the measured matrices for ATAA

ATAA							Statistical comparison		
	a	s_a	b (mL ng^{-1})	s_b (mL ng^{-1})	R^2 (%)	$s_{y/x}$	F_{calc}	t_{calc} (b)	t_{calc} (a)
Standard	580.42	965.04	728.54	18.75	99.8	1455.73			
HU	14.02	1136.31	749.78	22.07	99.74	1714.08	1.39	0.73	0.38
HM	−329.44	482.88	695.09	9.38	99.94	728.4	3.99	1.59	0.84
HF	1505.33	1259.14	704.96	24.46	99.64	1899.36	1.7	0.77	0.58
MU	−264.78	432.32	667.86	8.4	99.95	652.14	4.98	1.05	0.8
MM	578.4	611.66	680.24	11.88	99.91	922.67	2.49	2.18	0.01
MF	311.92	1155.73	729.4	22.45	99.72	1743.38	1.43	0.03	0.18
HDC	−481.05	613	688.52	11.91	99.91	924.68	2.48	1.8	0.93
HAL	−484.32	812.35	685.18	15.78	99.84	1225.4	1.41	1.77	0.84

Notes: a, intercept; s_a, intercept standard deviation; b, slope; s_b, slope standard deviation; R^2, determination coefficient; $s_{y/x}$, regression standard deviation. F_{tab} (df: 4; $p = 0.95$) = 6.38; t_{tab} (df: 10; $p = 0.95$) = 2.23.

Abbreviations: HU, human urine; HM, human microbial metabolome; HF, human feces; MU, mouse urine; MM, mouse microbial metabolome; MF, mouse feces; HDC, histidine decarboxylase activity; HAL, histidine ammonia-lyase activity.

every human and mouse sample, the absence of matrix effect was demonstrated. Therefore, the histidine metabolites should not present matrix effect in any of the matrices measured.

3.2.2 | Analytical characteristics of the method

Linearity of the curve calibration
Once the absence of matrix effect was demonstrated, a six point's calibration curve was built by injecting 100 μL of different standard solutions. A calibration curve for each histidine metabolite was constructed using analyte/internal standard peak-area ratio vs concentration of analyte. The results for the intercept (a), slope (b), correlation coefficient (R^2) and probability level of the lack-of-fit test, P_{lof} (%), are summarized in Table 4. The values of the correlation coefficients (R^2) ranged from 99.6 to 100% and p values were > 5% in all cases (P_{lof}%).[47] Thus, the data yield shows good linearity within the stated ranges.

Sensitivity (LOD and LOQ)
The values obtained for the LODs ranged from 0.2 to 2.4 ng mL^{-1}, and the LOQs from 0.7 to 8.2 ng mL^{-1} for *trans*-urocanate and imidazole-4-acetate, respectively. The results are summarized in Table 4.

Selectivity
The comparison between the chromatogram of a spiked sample containing a known concentration of the internal standards with the corresponding to the blank sample

demonstrated that they were not present in the samples, and interferences from endogenous substances were absent at the retention time of all analytes. Therefore, the optimized instrumental conditions confirmed a high selectivity of the proposed method. Chromatograms in MRM mode of a mouse fecal sample are shown in Figure 2 (HSS T3 column) and Figure 3 (BEH amide column).

Accuracy (trueness and precision)
We analyzed spiked samples at three concentration levels (5, 50, and 100 ng mL^{-1}) in three replicates for each compound in the solvent blank during three consecutive days. Precision was calculated as relative standard deviation (%RSD). Recovery rates (%Rec) were determined for trueness by comparing the estimated concentration with the spiked amount. Table 5 shows the results obtained. % Rec ranged from 87% for imidazole propionate to 114% for imidazole-4-acetate, which are within the recommended limits (±15% of nominal concentrations).[38] Inter-day precision was also <15% in all cases. Therefore, all compounds were within the acceptable limits for bioanalytical method validation.

3.3 | Biomonitoring of histidine bioactive metabolites in human and mouse urine, feces, and microbiota metabolome

L-histidine is a nutritionally essential amino acid with unique biochemical and physiological properties used to treat rheumatoid arthritis and anemia in patients with

TABLE 3 Matrix effect

Atenolol							Statistical comparison		
	a	s_a	b (mL ng^{-1})	s_b (mL ng^{-1})	R^2 (%)	$s_{y/x}$	F_{calc}	t_{calc} (b)	t_{calc} (a)
Standard	16224.03	9527.44	8530.31	185.08	99.86	14371.82			
HU	14208.95	8471.88	8622.77	164.57	99.89	12779.55	1.26	0.37	0.16
HM	−5217.72	7079.89	8793.32	137.53	99.93	10679.78	1.81	1.14	1.81
HF	14549.94	5085.34	8321	98.79	99.96	7671.06	3.51	1	0.16
MU	−584.73	6634.85	8862.22	128.89	99.94	10008.44	2.06	1.19	1.45
MM	−4418.15	8014.02	8754.45	155.68	99.91	12088.88	1.41	0.93	1.66
MF	11680.97	5728.56	8432.22	111.28	99.95	8641.34	2.77	0.45	0.41
HDC	2062.42	6856.23	8890.06	133.19	99.93	10342.39	1.93	1.58	1.21
HAL	−2797.81	7613.3	8829.67	147.89	99.92	11484.41	1.57	1.26	1.56

Notes: Comparison of calibration curves in H$_2$O + ACN (standard) and every of the measured matrices for atenolol. a, intercept; s_a, intercept standard deviation; b, slope; s_b, slope standard deviation; R^2, determination coefficient; $s_{y/x}$, regression standard deviation. F_{tab} (df: 4; $p = 0.95$) = 6.38; t_{tab} (df: 10; $p = 0.95$) = 2.23.

Abbreviations: HU, human urine; HM, human microbial metabolome; HF, human feces; MU, mouse urine; MM, mouse microbial metabolome; MF, mouse feces; HDC, histidine decarboxylase activity; HAL, histidine ammonia-lyase activity.

TABLE 4 Analytical and statistical parameters

	a	s_a	b	s_b	R^2 (%)	$s_{y/x}$	LOD (ng mL^{-1})	LOQ (ng mL^{-1})	P_{lof} (%)
HSS T3 column									
Histidine	−0.018	0.027	0.03	5.20×10^{-4}	99.9	0.04	1.4	4.8	12
N-acetylhistamine	0.714	0.401	0.635	7.80×10^{-3}	100	0.606	0.4	1.4	44
Glutamate	0.029	0.045	0.063	8.68×10^{-4}	99.9	0.067	1.5	5.2	27
Imidazole propionate	0.358	0.11	0.146	2.14×10^{-3}	99.9	0.166	0.8	2.6	33
Imidazole-4-acetate	−0.012	0.003	0.006	5.81×10^{-5}	100	0.005	2.4	8.2	35
Histamine	−0.042	0.007	0.008	1.45×10^{-4}	99.9	0.011	2.3	7.8	16
BEH amide column									
Cis-urocanate	0.273	0.517	0.304	1×10^{-2}	99.7	0.78	0.5	1.7	17
Trans-urocanate	−0.674	0.727	0.396	1.41×10^{-2}	99.6	1.097	0.2	0.7	20

Notes: n, points of calibration; *b*, slope; s_b, slope standard deviation; R^2, determination coefficient; $s_{y/x}$, regression standard deviation; LOD, limit of detection; LOQ, limit of quantification; P_{lof} (%), probability level of the *lack-of-fit* test.
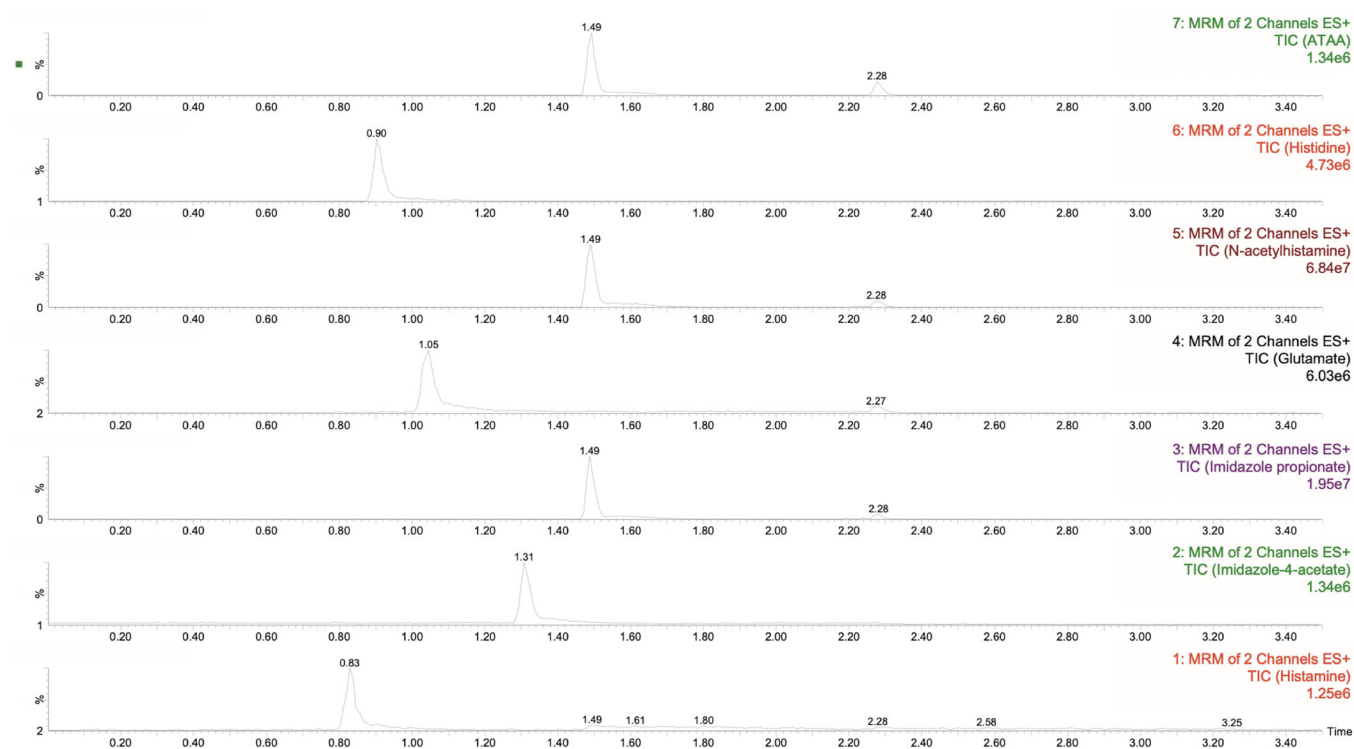

FIGURE 2 UHPLC–MS/MS chromatogram of a mouse sample with HSS T3 column

chronic renal failure in the past but recently investigated to prevent fatigue during strenuous exercise, as therapy in aging-related disorders, metabolic syndrome, atopic dermatitis, ulcers, inflammatory bowel diseases, ocular diseases, and neurological disorders and as biomarker of microbially-induced type II diabetes.[7,8,33] These effects are mediated by histidine and its major bioactive metabolites histamine, N-acetylhistamine, imidazole-4-acetate, *cis*-urocanate, *trans*-urocanate, glutamate, and imidazole propionate.[9–34,41] We developed and validated a simple, rapid and robust method to determine their concentrations in human and mice urine, feces and microbiota metabolome (Figure 4 and Table 6). The proposed method was applied to 10 human and 10 mice
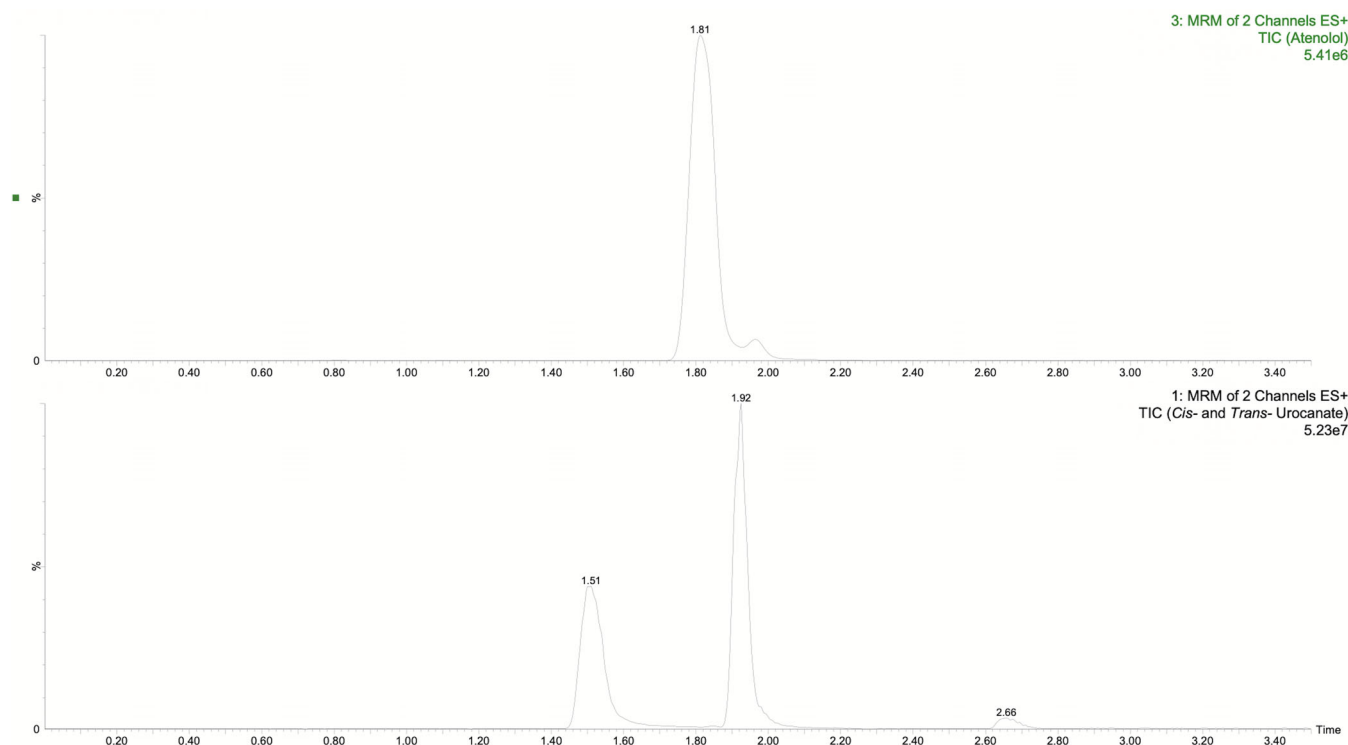
FIGURE 3 UHPLC–MS/MS chromatogram of a mouse sample with BEH amide column

samples. We also assessed production of *trans*-urocanate and histamine as result of HAL and HDC activities, the key enzymes governing histidine metabolic catabolism (Table S3).

All metabolites were quantified in mouse feces, suggesting broad exchange of histidine metabolites between the gut and the host. Glutamate and histamine were detected in all fluids and samples in concentrations ranging from 0.20 to 11.78 μM for glutamate and from 0.09 to 0.75 μM for histamine. The high frequency of detection of these metabolites is consistent with their central role in host metabolism and physiology. Mouse feces had the highest glutamate content 11.78 μM, 3.3 times higher than human feces, possibly linked to differences in gut microbiota composition between species.[48] Urine histamine levels in mice reached 0.75 μM, higher than those observed in human urine that were within previously published range.[49] Differences between species matrices was highlighted with histamine to histidine urine ratio that was 281 times higher in mice compared to humans, suggesting an underlying inflammatory or allergic process in our mice cohort.[13] The highest level of imidazole-4-acetate, the product of histamine oxidation by diamine oxidase and aldehyde dehydrogenase, was also observed in mouse urine, indicating a high catabolic rate of histamine. Mouse urine

also contained the highest amount of imidazole propionate among matrices, 10 times higher than in human urine. Imidazole propionate showed no association with infant health variables, possibly due to the low number of subjects. Conversely, N-acetylhistamine could only be quantified in human and mouse feces and in mouse urine at concentrations from 0.11 to 0.29 μM. The fact that N-acetylhistamine was detected in human and mouse feces confirmed previous reports on its origin from gut microbial metabolism[50] that can eventually be excreted in urine.[51]

Human urine had the highest concentration of histidine reaching 7.07 μM, possibly reflecting excessive dietary intake of histidine rather than impaired histidine degradation by HAL deficiency since its product *trans*-urocanate was detected in all urine samples. *Cis*-urocanate was effectively separated from *trans*-urocanate and quantified in all matrices but mouse urine, ranging from 0.01 μM in human feces and intracellular microbial metabolome to 0.07 μM in human urine. This finding likely results from UV exposure of the skin.[23] Finally, *trans*-urocanate reached the highest concentration (0.62 μM) in mouse feces as observed for glutamate, both metabolites being the initial and final intermediaries of histidine degradation pathway (Figure 1), indicating a high catabolic rate in mouse feces.

TABLE 5   Accuracy of the method

	Spiked (ng mL^{-1})	Found[a] (RSD) (ng mL^{-1})	Recovery (%)
Histidine	5	4.8 (3.2)	96
	50	48.2 (1.5)	96
	100	100.7 (2.8)	101
N-acetylhistamine	5	4.8 (3.8)	96
	50	48.8 (0.8)	98
	100	100.5 (3.5)	101
Glutamate	5	4.6 (3.9)	93
	50	49.2 (2.3)	98
	100	100.1 (3.1)	100
Imidazole propionate	5	4.3 (3.7)	87
	50	49.4 (1.7)	99
	100	99.9 (3.7)	100
Imidazole-4-acetate	5	5.7 (1.8)	114
	50	49.5 (0.3)	99
	100	100.5 (2.6)	101
Histamine	5	5.6 (0.8)	113
	50	48.7 (1.1)	97
	100	100.1 (2.6)	100
Cis-urocanate	5	4.4 (1.8)	88
	50	53.7 (0.5)	107
	100	98.6 (1)	99
Trans-urocanate	5	5.6 (0.3)	112
	50	52.1 (1.5)	104
	100	99.8 (0.7)	100

Notes: Recovery assay, precision, and trueness.
[a]Mean determination (relative standard deviation, %).

FIGURE 4   Histidine and its bioactive metabolites in biological samples: Human urine, human microbial metabolome, and human feces (HU, HM, and HF); and mouse urine, mouse microbial metabolome, and mouse feces (MU, MM, and MF). Averages across 10 replicates were used to determine the histidine metabolite contribution
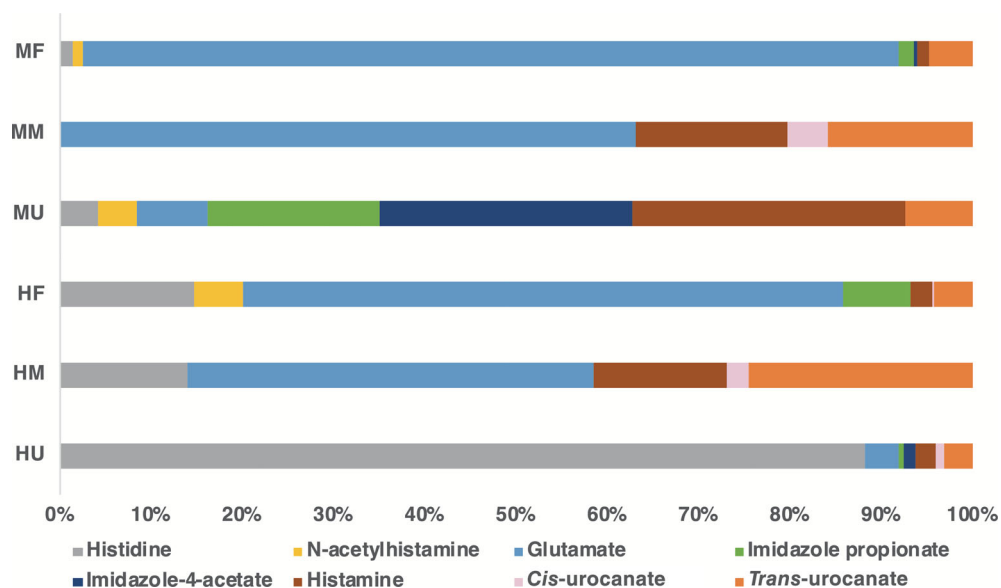
TABLE 6   Total histidine pool distribution (μmol L^{-1})

	Histidine	N-acetyl-histamine	Glutamate	Imidazole propionate	Imidazole-4-acetate	Histamine	Cis-urocanate	Trans-urocanate
HU	7.07 (6.02)	ND	0.31 (0.19)	0.04 (0.06)	0.1 (0.04)	0.18 (0.04)	0.07 (0.07)	0.25 (0.15)
HM	0.09 (0.08)	ND	0.29 (0.27)	ND	ND	0.09 (0.01)	0.01 (0.01)	0.16 (0.11)
HF	0.81 (0.34)	0.29 (0.47)	3.59 (2.86)	0.4 (0.36)	ND	0.13 (0.07)	0.01 (0.01)	0.23 (0.15)
MU	0.11 (0.02)	0.11 (0.06)	0.2 (0.05)	0.47 (0.39)	0.69 (0.32)	0.75 (0.75)	ND	0.18 (0.09)
MM	ND	ND	0.35 (0.44)	ND	ND	0.09 (0.01)	0.02 (0.04)	0.09 (0.13)
MF	0.2 (0.08)	0.13 (0.09)	11.78 (23.85)	0.22 (0.44)	0.04 (0.01)	0.16 (0.09)	0.02 (0.02)	0.62 (0.84)

Notes: Mean determination (SD). ND, not detected (<LOD).
Abbreviations: HU, human urine; HM, human microbial metabolome; HF, human feces; MU, mouse urine; MM, mouse microbial metabolome; MF, mouse feces.

4 | CONCLUSIONS

A precise quantitation of alterations in the histidine metabolism and its modulation by the microbiota is key to evaluate the impact of dysbiosis in neurological, immune, and metabolic diseases. Evaluation of histidine metabolites has been covered partially by several separate methods with varying scope, sensitivity and accuracy, preventing simultaneous quantitation and association of metabolites and ratios with histidine related disorders. To fill this gap, we have developed and validated a rapid, robust, high-throughput method for quantitation of histidine and seven bioactive metabolites easily extracted from human and mice urine, feces, and microbiota metabolome using liquid chromatography–tandem mass spectrometry. Despite target compounds had different physicochemical properties, we managed to simultaneously measure histidine metabolites with a 6.5 min run time. Our novel approach captures histidine metabolism in a single assay with a high level of accuracy and reproducibility, making it especially interesting for deep microbiota metabolic phenotyping in large disease studies and postnatal routinely screening of alterations in histidine pathway.

CONFLICT OF INTEREST

The authors declare that they have no competing interest.

DATA AVAILABILITY STATEMENT

The data that support the findings of this study are available from the corresponding author upon reasonable request.

ORCID

Inmaculada Acuña 🔾 https://orcid.org/0000-0002-1265-770X
Margarita Aguilera 🔾 https://orcid.org/0000-0002-3204-9787

REFERENCES

1. Farag MA, Abdelwareth A, Sallam IE, el Shorbagi M, Jehmlich N, Fritz-Wallace K, et al. Metabolomics reveals impact of seven functional foods on metabolic pathways in a gut microbiota model. J Adv Res. 2020;23:47–59.
2. Rinninella E, Raoul P, Cintoni M, Franceschi F, Miggiano GAD, Gasbarrini A, et al. What is the healthy gut microbiota composition? A changing ecosystem across age, environment, diet, and diseases. Microorganisms. 2019;7:14.
3. Zheng X, Xie G, Zhao A, Zhao L, Yao C, NHL C, et al. The footprints of gut microbial–mammalian co-metabolism. J Proteome Res. 2011;11:5512–22.
4. Agus A, Planchais J, Sokol H. Gut microbiota regulation of tryptophan metabolism in health and disease. Cell Host Microbe. 2018;23:716–24.
5. Yano JM, Yu K, Donaldson GP, Shastri GG, Ann P, Ma L, et al. Indigenous bacteria from the gut microbiota regulate host serotonin biosynthesis. Cell. 2015;161:264–76.
6. Chen H, Nwe P-K, Yang Y, Rosen CE, Bielecka AA, Kuchroo M, et al. A forward chemical genetic screen reveals gut microbiota metabolites that modulate host physiology. Cell. 2019;177:1217–1231.e18.
7. Moro J, Tome D, Schmidely P, Demersay T, Azzout-Marniche D. Histidine: a systematic review on metabolism and physiological effects in human and different animal species. Nutrients. 2020;12:1–20.

8. Brosnan ME, Brosnan JT. Histidine metabolism and function. J Nutr. 2020;150:2570S–5S.

9. Kopple JD, Swendseid ME. Evidence that histidine is an essential amino acid in normal and chronically uremic man. J Clin Investig. 1975;55:881–91.

10. DiNicolantonio JJ, McCarty MF, OKeefe JH. Role of dietary histidine in the prevention of obesity and metabolic syndrome. Open Heart. 2018;5:e000676.

11. Schubert ML, Peura DA. Control of gastric acid secretion in health and disease. Gastroenterology. 2008;134:1842–60.

12. Hu W, Chen Z. The roles of histamine and its receptor ligands in central nervous system disorders: an update. Pharmacol Therap. 2017;175:116–32.

13. Branco ACCC, Yoshikawa FSY, Pietrobon AJ, Sato MN. Role of histamine in modulating the immune response and inflammation. Mediators Inflamm. 2018;2018:1–10.

14. Pugin B, Barcik W, Westermann P, Heider A, Wawrzyniak M, Hellings P, et al. A wide diversity of bacteria from the human gut produces and degrades biogenic amines. Microbial Ecol Health Dis. 2017;28:1353881.

15. Valembois S, Krall J, Frølund B, Steffansen B. Imidazole-4-acetic acid, a new lead structure for interaction with the taurine transporter in outer blood-retinal barrier cells. Eur J Pharm Sci. 2017;103:77–84.

16. Krall J, Brygger BM, Sigurðardóttir SB, Ng CKL, Bundgaard C, Kehler J, et al. Discovery of α-substituted imidazole-4-acetic acid analogues as a novel class of ρ1γ-aminobutyric acid type A receptor antagonists with effect on retinal vascular tone. ChemMedChem. 2016;11:2299–310.

17. Chu Z, Liu P, Li X, Liu Y, Liu F, Lei G, et al. Microinjection of valproic acid into the ventrolateral orbital cortex exerts an antinociceptive effect in a rat of neuropathic pain. Psychopharmacology (Berl). 2020;237:2509–16.

18. Tunnicliff G. Pharmacology and function of imidazole 4-acetic acid in brain. Gen Pharmacol. 1998;31:503–9.

19. Canadian Institutes of Health Research, Canada Foundation for Innovation, and by T. M. I. C. (TMIC). The human metabolome database. N-Acetylhistamine; 2019.

20. Hart PH, Norval M. The multiple roles of urocanic acid in health and disease. J Investig Dermatol. 2020;141:496–502.

21. Zhu H, Wang N, Yao L, Chen Q, Zhang R, Qian J, et al. Moderate UV exposure enhances learning and memory by promoting a novel glutamate biosynthetic pathway in the brain. Cell. 2018;173:1716–1727.e17.

22. Stipanuk MH, Caudill MA. Biochemical, physiological, & molecular aspects of human nutrition. 4th ed. St. Louis, MO: Elsevier/Saunders; 2006.

23. Korhonen E, Bisevac J, Hyttinen JMT, Piippo N, Hytti M, Kaarniranta K, et al. UV-B-induced inflammasome activation can be prevented by cis-urocanic acid in human corneal epithelial cells. Investig Ophthalmol Vis Sci. 2020;61:7.

24. Menezes AC, Raposo S, Simões S, Ribeiro H, Oliveira H, Ascenso A. Prevention of photocarcinogenesis by agonists of 5-HT1A and antagonists of 5-HT2A receptors. Mol Neurobiol. 2016;53:1145–64.

25. Albert E, Walker J, Thiesen A, Churchill T, Madsen K. Cis-urocanic acid attenuates acute dextran sodium sulphate-induced intestinal inflammation. PLoS One. 2010;5:e13676.

26. Correale J, Farez MF. Modulation of multiple sclerosis by sunlight exposure: role of cis-urocanic acid. J Neuroimmunol. 2013;261:134–40.

27. Bukke VN, Archana M, Villani R, Romano AD, Wawrzyniak A, Balawender K, et al. The dual role of glutamatergic neurotransmission in Alzheimer's disease: from pathophysiology to pharmacotherapy. Int J Mol Sci. 2020;21:1–29.

28. Li W, Kutas M, Gray JA, Hagerman RH, Olichney JM. The role of glutamate in language and language disorders—evidence from ERP and pharmacologic studies. Neurosci Biobehav Rev. 2020;119:217–41.

29. Ibrahim KS, Abd-Elrahman KS, El Mestikawy S, Ferguson SSG. Targeting vesicular glutamate transporter machinery: implications on metabotropic glutamate receptor 5 signaling and behavior. Mol Pharmacol. 2020;98:314–27.

30. Fischer KD, Knackstedt LA, Rosenberg PA. Glutamate homeostasis and dopamine signaling: implications for psychostimulant addiction behavior. Neurochem Int. 2021;144:104896.

31. Hodo TW, de Aquino MTP, Shimamoto A, Shanker A. Critical neurotransmitters in the Neuroimmune network. Front Immunol. 2020;11:1–26.

32. Molinaro A, Bel Lassen P, Henricsson M, Wu H, Adriouch S, Belda E, et al. Imidazole propionate is increased in diabetes and associated with dietary patterns and altered microbial ecology. Nat Commun. 2020;11:5881.

33. Koh A, Molinaro A, Ståhlman M, Khan MT, Schmidt C, Mannerås-Holm L, et al. Microbially produced imidazole propionate impairs insulin signaling through mTORC1. Cell. 2018;175:947–961.e17.

34. Koh A, Mannerås-Holm L, Yunn NO, Nilsson PM, Ryu SH, Molinaro A, et al. Microbial imidazole propionate affects responses to metformin through p38γ-dependent inhibitory AMPK phosphorylation. Cell Metabol. 2020;32:643–653.e4.

35. Illig T, Gieger C, Zhai G, Römisch-Margl W, Wang-Sattler R, Prehn C, et al. A genome-wide perspective of genetic variation in human metabolism. Nat Genet. 2009;42:137–41.

36. Kammeyer A, Pavel S, Asghar SS, Bos JD, Teunissen MBM. Prolonged increase of cis-urocanic acid levels in human skin and urine after single total-body ultraviolet exposures. Photochem Photobiol. 1997;65:593–8.

37. Berglund SK, García-Valdés L, Torres-Espinola FJ, Segura MT, Martínez-Zaldívar C, Aguilar MJ, et al. Maternal, fetal and perinatal alterations associated with obesity, overweight and gestational diabetes: an observational cohort study (PREOBE). BMC Public Health. 2016;16:207.

38. U.S. Department of Health and Human Services, Food and Drug Administration, Center for Drug Evaluation and Research (CDER), Center for Veterinary Medicine (CVM). Bioanalytical method validation. Guidance for Industry; 2018. https://www.fda.gov/files/drugs/published/Bioanalytical-Method-Validation-Guidance-for-Industry.pdf (Accessed January 26, 2021).

39. Currie LA. Detection and quantification limits: origins and historical overview. Anal Chim Acta. 1999;391:127–34.

40. Lin R, Liu W, Piao M, Zhu H. A review of the relationship between the gut microbiota and amino acid metabolism. Amino Acids. 2017;49:2083–90.

41. Torii K, Uneyama H, Nakamura E. Physiological roles of dietary glutamate signaling via gut-brain axis due to efficient digestion and absorption. J Gastroenterol. 2013;48:442–51.

42. Tolstikov VV, Fiehn O. Analysis of highly polar compounds of plant origin: combination of hydrophilic interaction chromatography and electrospray ion trap mass spectrometry. Anal Biochem. 2002;301:298–307.

43. Joo KM, Han JY, Son ED, Nam GW, Chung HY, Jeong HJ, et al. Rapid, simultaneous and nanomolar determination of pyroglutamic acid and *cis-/trans*-urocanic acid in human stratum corneum by hydrophilic interaction liquid chromatography (HILIC)-electrospray ionization tandem mass spectrometry. J Chromatogr B Analyt Technol Biomed Life Sci. 2012;897:55–63.

44. Silvestro L, Tarcomnicu I, Rizea S. Matrix effects in mass spectrometry combined with separation methods — comparison HPLC, GC and discussion on methods to control these effects. In: Coelho AV (Ed.), Tandem Mass Spectrom. –Mol. Charact, InTech, 2013. Available online: https://www.intechopen.com/books/tandem-mass-spectrometry-molecular-characterization/matrix-effects-in-mass-spectrometry-combined-with-separation-methods-comparison-hplc-gc-and-discussi (Accessed December 9, 2020).

45. Trufelli H, Palma P, Famiglini G, Cappiello A. An overview of matrix effects in liquid chromatography–mass spectrometry. Mass Spectrom Rev. 2011;30:491–509.

46. Cantarero S, Zafra-Gomez A, Ballesteros O, Navalon A, Vilchez JL, Verge C, et al. Matrix effect study in the determination of linear alkylbenzene sulfonates in sewage sludge samples. Environ Toxicol Chem. 2011;30:813–8.

47. Analytical Methods Committee. Is my calibration linear? Analyst. 1994;119:2363–6.

48. Liu R, Hong J, Xu X, Feng Q, Zhang D, Gu Y, et al. Gut microbiome and serum metabolome alterations in obesity and after weight-loss intervention. Nat Med. 2017;23:859–68.

49. Myers G, Donlon M, Kaliner M. Measurement of urinary histamine: development of methodology and normal values. J Allergy Clin Immunol. 1981;67:305–11.

50. Fujisaka S, Avila-pacheco J, Soto M, Kostic A, Dreyfuss JM, Pan H, et al. Diet, genetics, and the gut microbiome drive dynamic changes in plasma metabolites. Cell Rep. 2018;22:3072–86.

51. Van Der Heiden C, Wadman SK, De Bree PK, Wauters EAK. Increased urinary imidazolepropionic acid, n-acetylhistamine and other imidazole compounds in patients with intestinal disorders. Clin Chim Acta. 1972;39:201–14.

SUPPORTING INFORMATION

Additional supporting information may be found online in the Supporting Information section at the end of this article.